

Thermal evolution of Mercury: implication for despinning and contraction.

Guillaume Robuchon¹, Gabriel Tobie^{1,2}, Gael Choblet^{1,2}, Ondrej Čadek³ and Antoine Mocquet^{1,2}. ¹Laboratoire de Planétologie et Géodynamique, Université de Nantes, France, ²UMR-6112, CNRS, Nantes, France and ³Department of Geophysics, Faculty of Mathematics and Physics, Charles University, Prague, Czech Republic

Introduction. Mercury's surface exhibits specific compressive features, called lobate scarps [1], that suggest that Mercury has experienced a change of shape during its history (e.g [3]). These compressive features indicate global contraction and their apparent N-S preferred orientation suggest a possible effect of tidal despinning [10]. Both despinning and contraction result from the interior evolution. The timing of the decrease in Mercury's rotation rate is not clearly established. The analysis of the terrains associated to the lobate scarps provide evidences for a formation after the end of Late Heavy Bombardment (LHB) [2]. The lack of a strong latitudinal dependence of these lobate scarps however indicates that despinning occurs prior to the end of LHB, ancient tectonic features being erased by the end of LHB.

By adapting a model initially developed for Iapetus ([13]), here we propose to evaluate the thermal evolution of Mercury and the associated despinning and contraction, particularly during the early stage before LHB. We perform 3D numerical simulations for a wide range of plausible initial conditions to evaluate: (1) the evolution of the temperature structure, (2) the resulting despinning rate, (3) the change of Mercury's shape and (4) the associated lithospheric stress field.

Thermal evolution. Thermal convection equations are solved for a fluid with temperature-dependent viscosity in a spherical geometry (Fig. 1), using the numerical tool OEDIPUS [8] in order to describe the thermal evolution of the silicate mantle. The mantle viscosity is assumed to be dominated by diffusion creep in dry olivine [6]. Different values for the activation energy, E_a , ranging from 230 to 300 kJ.mol⁻¹ are considered, and the pressure dependency is neglected. A uniform temperature of 440 K is prescribed at the surface while the bottom temperature is consistently determined from the energy budget of the metallic core. Cooling and crystallization of the core is computed for sulfur contents ranging from 2 to 4 % following [15]. As an initial condition, an isothermal mantle is considered with temperature T_{init} ranging from 1500 to 2100 K. The initial temperature at the CMB is set to 2100K. The surface temperature is kept constant throughout the evolution. Before 100 Myr, both a cold and a hot boundary layers develop at the top and at the bottom of the mantle respectively (Fig. 2). The first convective instability occurs within the hot bottom boundary layer at 300 Myr. Note that the inner core starts crystallizing at ~180 Myr, before the onset of convection. The

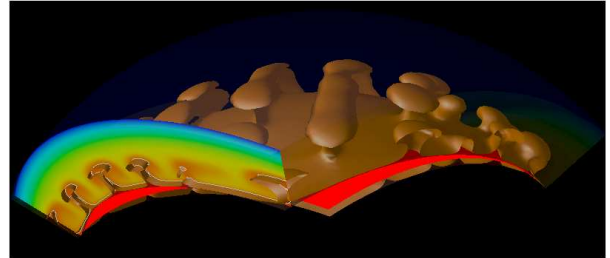


Figure 1: Snapshot of a typical run showing a large number of upwellings. Only one of the six blocks is displayed. The isosurface corresponds to the 1950 K isotherm. For this simulation the initial values are $T_{init} = 1700$ K, $E_a = 261$ kJ.mol⁻¹ and $S = 2$ %.

growth rate of the inner core is enhanced by the increase of CMB heat flux caused by convection. The vigour of convection progressively decays after 2 billion years and the conductive lid thickens.

For T_{init} varying between 2100 and 1500 K, the onset time ranges from 220 to 890 Myr. For the hotter cases the convection-induced acceleration of the inner core growth thus occurs before LHB while for the colder cases this acceleration occurs after LHB. This may have important implication for timing of global contraction. In all the performed simulations convective motions still operate at 5 billion years (the typical duration of our numerical experiments).

Implication for despinning and contraction. The horizontally averaged temperature profiles and the radius of inner core obtained from the 3D internal model as a function of time can be used to compute the evolution of Mercury's rotation and shape. The despinning rate due to tidal dissipation of the rotational energy in the interior is computed using the method of [13] adapted from [16] and [14]. For sake of simplicity, the orbital eccentricity is neglected and there is no differential rotation between the solid mantle and the liquid core. Two rheological models are considered: (1) a simple Maxwell model, (2) a generalized Burgers model initially developed to explain the seismic attenuation data for the Earth's upper mantle [9]. For the Faul and Jackson model, uniform grain sizes of 1 and 10 mm are used. Following [10], an initial rotation period of 20 hours is used.

When a Maxwell rheology is assumed, despinning is not

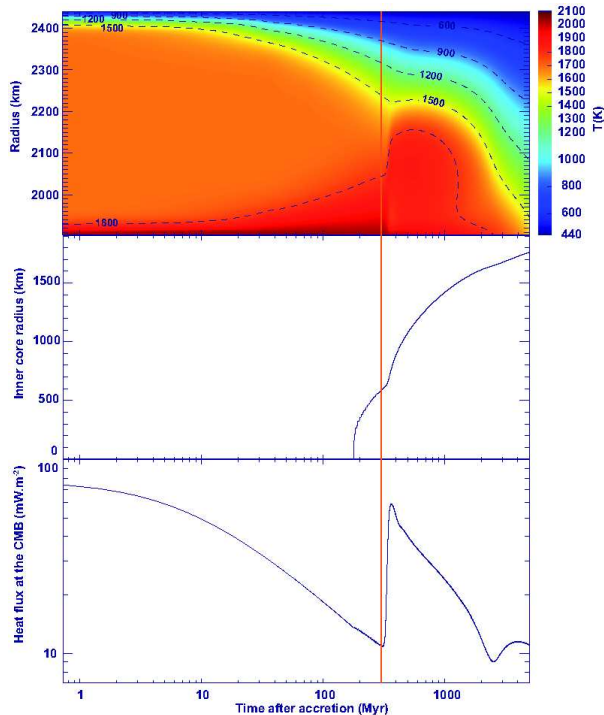


Figure 2: Time evolution for the simulation displayed on Fig. 1.

obtained in any of our simulations. Despinning is only observed when the Faul and Jackson model is considered. The despinning is completed at 72 Myr and 119 Myr for grain sizes of 1 and 10 mm, respectively (Fig. 3). The dissipation factor Q typically ranges between 10 and 70. For the two values of the grain size considered here, the evolution of Q displays opposite tendencies. For all the simulations tested, despinning is completed before the LHB and before the onset of convection.

Computation of the shape evolution requires to consider simultaneously the degree-two change due to despinning and the radial contraction. The latter process is controlled by density variations due to both the crystallization of the inner core and the thermal evolution of the mantle and to a lesser extent by the reduction of the centrifugal forces. The adjustment of the shape is then controlled by the visco-elastic properties of the mantle.

The final goal of our study is to self-consistently compute these different effects using the spectral approach developed by [11] and [12]. These numerical developments are currently in progress. These will provide reference stress fields for various interior models that can be compared to the map of tectonic structures currently revealed

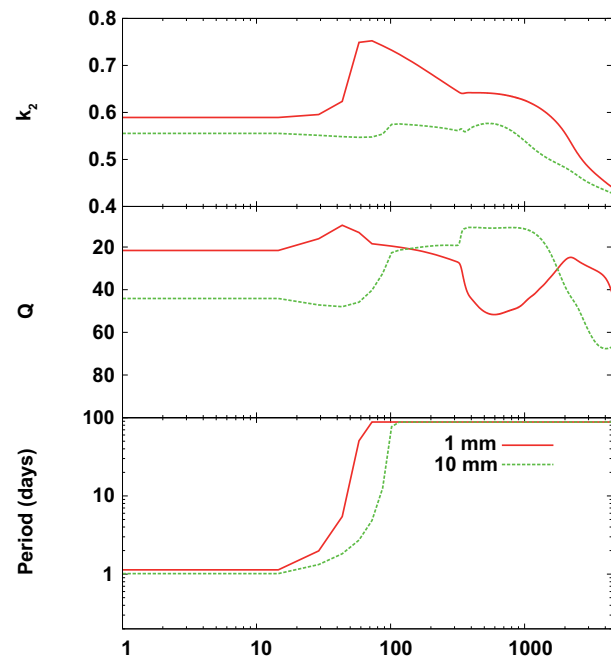


Figure 3: Evolution of the tidal Love number k_2 , the dissipation factor Q and the rotation period. Same parameter as Fig. 2

by Messenger, thus leading to further insights in the evolution of Mercury.

References

- [1] R. G. Strom et al (1975). *J. Geophys. Res.*, 80, 2478–2507.
- [2] T. R. Watters et al (1998). *Geology*, 26, 991–994.
- [3] A. J. Dombard and S. A. Hauck II. (2008) *Icarus*, 198, 274–276.
- [4] Hauck et al (2004) *Earth Planet. Sci. Lett.*, 222, 713–728.
- [5] R. Gomes et al (2005). *Nature*, 435, 466–469.
- [6] Korenaga, J. and Karato, S. (2008) *J. Geophys. Res.*, 113, 2403
- [7] G. Choblet (2005). *J. Comput. Phys.*, 205, 269–291.
- [8] G. Choblet et al (2007). *Geophys. J. Int.*, 170, 9–30.
- [9] U. H. Faul and I. Jackson (2005). *Earth Planet. Sci. Lett.*, 234, 119–134.
- [10] H. J. Melosh and D. Dzurisin (1978). *Icarus*, 35, 227–236.
- [11] O. Cadek (2003). In *EGS-AGU-EUG*, 5279.
- [12] G. Tobie et al (2008). *Icarus*, 196, 642–652.
- [13] G. Robuchon et al (2009). *Icarus*, submitted.
- [14] G. Tobie et al (2005). *Icarus*, 177, 543–549.
- [15] G. Schubert et al (1988). in *Mercury*, 429–460.
- [16] S.J. Peale et al (1979). *Science*, 203, 892–894.